Aerodynamic Benefits of Camber Morphing Technology for Strut-Braced Wing Configurations

Tsatsas, I.; Sticchi, E.; Carrillo Córcoles, X.; De Breuker, R.; Sodja, J.

DOI
10.2514/6.2025-0281

Publication date
2025

Document Version
Final published version

Published in
Proceedings of the AIAA SCITECH 2025 Forum

AIAA SciTech Forum
6-10 January 2025, Orlando, FL
AIAA SCITECH 2025 Forum

10.2514/6.2025-0281

Aerodynamic Benefits of Camber Morphing Technology for Strut-Braced Wing Configurations

Ilias Tsatsas*, Emanuele Sticchi†, Xavier Carrillo Córcoles‡, Roeland De Breuker§ and Jurij Sodja¶
Delft University of Technology, Faculty of Aerospace Engineering, Kluyverweg 1, Delft, 2629 HS, The Netherlands

This study investigates the aerodynamic benefits of integrating trailing edge camber morphing on the strut of a regional strut-braced wing aircraft designed to cruise at Mach number of 0.5. Strut-braced wings are recognized for their weight advantages in high aspect ratio designs compared to the equivalent cantilever wings since the strut decreases the main wing's bending moment. Hence, the induced drag component can be reduced due to the high aspect ratio without increasing the weight of the main wing. However, the strut increases the parasite drag component highlighting the need for innovative methods to improve the strut-braced wing overall aerodynamic efficiency. Recent studies have shown the significance of strut shape in the overall drag reduction and the necessity of maintaining high aerodynamic efficiency in off-design conditions. In this work, a genetic algorithm was utilized in conjunction with a mid-fidelity aerodynamic model to optimize the morphing strut trailing edge geometry across a range of climb and cruise conditions. The optimization objective was the minimization of drag and the design variables were the equivalent trailing edge deflection angles in seven sections of the strut. The results demonstrate a drag reduction of 0.5% to 3% both in climb and cruise. For lift coefficients below 0.8, the drag reduction is mainly attributed to the redistribution of the loading and the induced drag component reduction. In contrast, at lift coefficients above 0.8, the parasite drag component decreases due to the increased region of laminar flow over the upper wing surface.

I. Nomenclature

Λ	=	sweep angle
α	=	angle of attack
δ_{TE}	=	equivalent trailing edge deflection angle
C_{D_i}	=	global (strut and wing) induced drag coefficient
C_{D_p}	=	global parasite drag coefficient
C_f	=	friction drag coefficient
C_L	=	global lift coefficient
C_p	=	pressure coefficient
M	=	Mach number
S	=	wing surface
b	=	wing span
c_{d_p}	=	sectional profile drag coefficient
c_l^{st}	=	strut sectional lift coefficient
c_l^w	=	wing sectional lift coefficient
c_l	=	sectional lift coefficient

*PhD Candidate, Faculty of Aerospace Engineering, Aerospace Structures and Materials, Kluyverweg 1, 2629 HS, Delft, i.tsatsas@tudelft.nl
†PhD Candidate, Faculty of Aerospace Engineering, Flow Physics and Technology, Kluyverweg 1, 2629 HS, Delft, e.sticchi@tudelft.nl
‡Researcher, Faculty of Aerospace Engineering, Aerospace Structures and Materials, Kluyverweg 1, 2629 HS, Delft, x.carrillocorcoles@tudelft.nl
§Associate Professor, Faculty of Aerospace Engineering, Aerospace Structures and Materials, Kluyverweg 1, 2629 HS, Delft, r.debreuker@tudelft.nl, AIAA Associate Fellow
¶Assistant Professor, Faculty of Aerospace Engineering, Aerospace Structures and Materials, Kluyverweg 1, 2629 HS, Delft, j.sodja@tudelft.nl, AIAA Senior Member

c_{st} = strut chord
c_w = wing chord

II. Introduction

The Truss-Braced Wing (TBW) layout is currently considered one of the most feasible candidate for increasing medium-range commercial aircraft efficiency among other unconventional aircraft configurations including blended-wing-body, twin fuselage, and flying-V [1, 2]. A full-scale demonstrator with the TBW configuration, known as X-66, is scheduled for its maiden flight in 2028 by NASA and Boeing [3]. TBW is a variant of the joint-wing concept, in which the wing is usually connected to the upper part of the fuselage and the strut starts at the lower part of the fuselage and ends around the wing's half-span. Sometimes, smaller jury struts connect the wing and the strut [4]. If no jury struts are implemented, the layout is called Strut-Braced Wing (SBW).

The primary purpose of the TBW concept is to enable slender high-aspect-ratio wings (HARW) with an extended span, which contributes to reduce lift-induced drag [2], without significantly adding weight to the wing structure. Pfenninger [5] was the first to introduce the idea of SBW in the wider context of Laminar Flow Control (LFC). He envisioned that the strut support could reduce the thickness of the main wing, and therefore reduce the wave drag in high speeds [6]. As a result, the sweep angle could be reduced and when combined with the smaller chord of an HARW, this design could lower the Reynolds number and offer a more suitable planform for LFC [5]. However, the strut generates both its own viscous drag and interference drag with the main wing, hence, a laminarized strut was perceived as the only solution to overcome these drag penalties during the 1980s [7]. Further studies on interference drag in the transonic regime, revealed that it is primarily influenced by the junction angle and the strut's thickness-to-chord ratio [8, 9]. At the time, the SBW was also considered less productive than the CTW due to its expected higher manufacturing costs and lower cruise speeds [10].

The presence of the strut decreases the wing root bending moment compared to the traditional Cantilever Wing (CTW) [6]. However, its weight is added to the total weight and due to its tendency to buckle at -1.0g and -2.0g loads, its weight can increase significantly [11]. To address this problem, Gern et al. [1] performed a Multidisciplinary Design Optimization (MDO) of a SBW long-range transport aircraft, proposing a telescoping strut with a damping mechanism to reduce strain under negative loads, thereby avoiding the strut's weight increase. More recent studies at Virginia Tech have also shown that SBW design can increase the efficiency of military cargo [12] and medium-range transport aircraft [6], even with a non-telescopic strut. NASA extended the research on SBW through the SUGAR project [13], where the aerodynamic analysis was initially performed with the Vortex Lattice Method (VLM)[14].

High-fidelity tools have also been used to perform the aerodynamic optimization of SBW configuration [15]. First, Secco and Martins [16] applied Computational Fluid Dynamics (CFD) with an overset mesh and Reynolds-Averaged Navier-Stokes (RANS) models, finding that drag reduction was more effectively achieved by altering the strut's shape rather than the main wing's shape. Second, Chau and Zingg [17] similarly implemented RANS-based optimization and noticed that the SBW may operate more efficiently in cruise conditions characterized by a higher lift coefficient, hence, at higher cruise altitude than the typical, in order to balance levels of induced and parasite drag. Their main findings were that strut shape should change from positive lift near the root to negative near the junction and that fuel savings are higher when operating over long ranges in high wing loading conditions. Consequently, they proposed investigating performance changes across a range of cruise and climb conditions [17].

Given the requirements for strut shape changes and the increase of the SBW efficiency across a range of conditions, the morphing technology application to the strut is examined in this paper. According to Li et al. [18], the main goal of the morphing concept is to provide structures that are able to change their shape ("morphi" in Greek) in a continuous and seamless manner [19]. The continuous smooth change in the camber of a morphed trailing edge (TE) improves significantly (50%) the lift to drag ratio when compared to hinged flaps deflected at high angles (15°- 20°) as shown in the results of Rivero et al., since it prevents the development of the bluff body-like vortex sheet [20]. The seamless transition prevents tip vortex formation at the edges of the conventionally hinged deflected surfaces, thus, the aerodynamic efficiency increases via a rise in the pressure coefficient and a drop in the friction coefficient [21]. Moreover, the absence of recirculation areas around these gaps promotes the laminarity of the flow [22].

Therefore, this paper examines the potential benefits that the integration of the morphing technology to the TE of the strut could have on the overall aerodynamic efficiency of a SBW configuration. Section III presents the morphing concept realization, the aerodynamic model and the optimization algorithm that were used to find the optimum strut TE shapes in each condition. Then, Section IV presents the optimization results and the associated drag benefits. Finally, the main conclusions are outlined in Section V.

III. Methodology

This section begins with the description of the trailing edge morphing implementation. Next, the Quasi-Three-Dimensional (Q3D) aerodynamic model used to assess the aerodynamic efficiency benefits of the morphing strut is presented. Then, the optimization process is described including the objective function, the variables and their constraints.

A. Morphing Strut Concept

Many morphing concepts have been recommended in the literature such as variable airfoil camber and thickness, as well as variable wing twist, span and sweep [18]. However, the susceptibility of the strut box to buckling under negative loads [11] prevents the consideration of variable thickness mechanisms. In addition, the span and sweep variations of the strut are constrained because it is connected to the wing. Hence, only the leading and trailing edge morphing mechanisms can be examined. Moreover, the aerodynamic loads on the leading edge (LE) are expected to be higher due to the suction peak in this region [23], therefore, greater actuation forces would be required, which would increase the volume of actuators in the already limited space of strut. Therefore, only the camber morphing through the trailing edge (TE) deflection is investigated in this paper.

The camber morphing concept considered in this work is based on the Translation Induced Camber (TRIC) concept that was developed at the TU Delft [24]. Initially, Vos et al. [25] proposed adding a discontinuity at the trailing edge to reduce its torsional stiffness and a threaded rod to introduce relative spanwise movement between the upper and lower skins, hence, twist. Then, Werter et al. [23] suggested the implementation of actuators in chordwise direction to enable both bending if they move in the same direction and twist if they move differentially.

Next, Mkhoyan et al. [26] proposed a distributed philosophy of independent morphing, seamlessly connected with elastomeric segments to simultaneously control the attitude (pitch, roll, yaw), the aeroelastic behavior (load alleviation, flutter control) of the aircraft and enable continuous performance optimization in off-design conditions. This study now explores the application of the TRIC concept distributed along the straight part of the strut (as highlighted in red in Fig. 1a) in order to reduce the drag of SBW configurations.

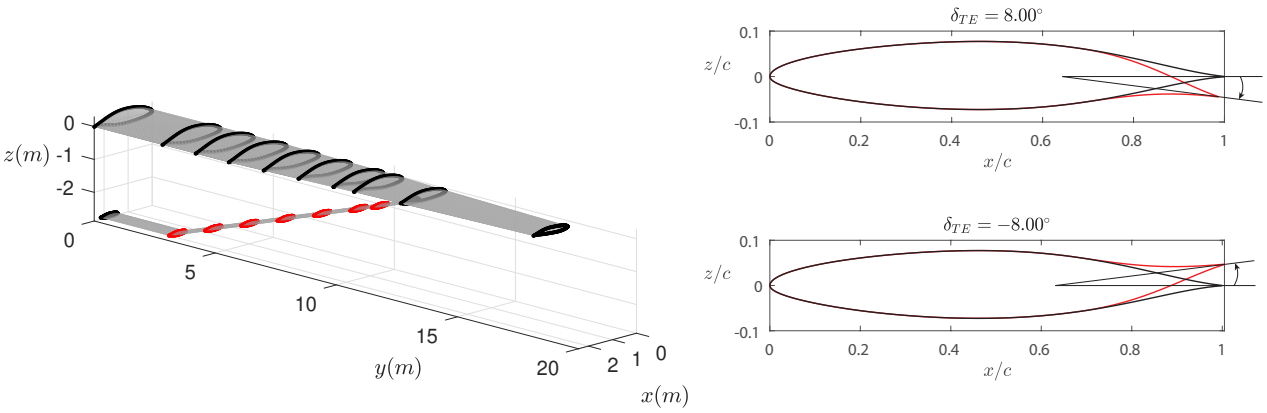

(a) SBW geometry - morphing sections (red), passive (black) **(b) Morphing shape and deflection angle limits**

Fig. 1 Morphing shapes geometry and location

In order to create and optimize the TE morphing shape, a parametrization method is needed. Derksen and Rogalsky [27] propose a parametrization of airfoils with two 4th-order Bezier curves, one for the camber line and one for the thickness distribution. Since only the strut's TE shape optimization was considered in this study, a similar parametrization was developed, in which the two 4th-order polynomials were used to describe the airfoil from the rear spar to the TE, while the upstream section remained unchanged. Using these polynomials, the TE geometry was fully described by 10 parameters.

However, when the design constraints of the TRIC concept [24] were taken into account, such as the constant length of the top skin, the smooth transition from the main airfoil to the morphing TE part and structural considerations like curvature limits of the skin, the TE camber morphing could be fully defined by a single parameter, the equivalent trailing

edge deflection angle, δ_{TE}. This angle, δ_{TE}, is defined as the angle formed between the undeformed chord line and the line connecting the midpoint of the rear spar with the trailing edge (TE) point, as Fig. 1b indicates.

B. Aerodynamic Model

The objective of the aerodynamic analysis was to investigate the effect of a camber morphing strut on the overall SBW aerodynamic efficiency across a typical mission, aiming to reduce the total fuel burn. Two main segments were identified: climb and cruise. To make the optimization feasible from a computational cost perspective, a rapid aerodynamic tool was required. Previous experience has shown that although Q3D methods often underpredict the parasite drag compared to high-fidelity 3-D tools, they effectively capture the lift distribution and the induced drag component. Therefore, they are sufficient for optimization purposes [28].

Hence, a Q3D solver incorporating Athena Vortex Lattice (AVL) [29] and MSES software [30], as established by Mariens et al. [31] and later modified for SBW applications by Sticchi et al. [32] was adopted and extended in this work to include the camber morphing strut concept. The main goal was to minimize drag by optimizing the morphing shape of the strut. To achieve this, specific 2-D sections of the strut were selected for optimization. The global lift distribution and the induced drag were calculated by AVL, while MSES accounted for the 2-D sectional profile drag of the selected sections.

Initially, the spanwise lift distribution of the whole SBW was calculated with AVL for a given total lift coefficient, C_L. AVL assumes that the flow is inviscid, incompressible and irrotational [14], hence, it should only be applied to thin lifting surfaces at small angles of attack and sideslip. Moreover, compressibility effects are accounted for Mach<0.6 by the Prandtl-Glauert (PG) correction factor [29]. Therefore, AVL can be used to calculate the C_L and the induced drag coefficient, C_{D_i} of the SBW on cruise and climb conditions.

To verify this assumption, the C_L versus α diagrams were produced for both climb and cruise using AVL and compared against the CFD data of the same SBW with passive (non-morphing) strut that were available from [32]. Figure 2 shows that in the conditions of interest the $C_L - \alpha$ curve is linear. As a result, the AVL outputs for C_L and C_{D_i} which mainly depends on lift distribution, can be considered reliable. However, AVL cannot capture the profile drag components [14] comprising pressure (form) drag and skin friction drag [33]. For this reason, the local or sectional lift coefficients, c_l corresponding to specific spanwise positions were calculated with AVL and then, fed into the MSES.

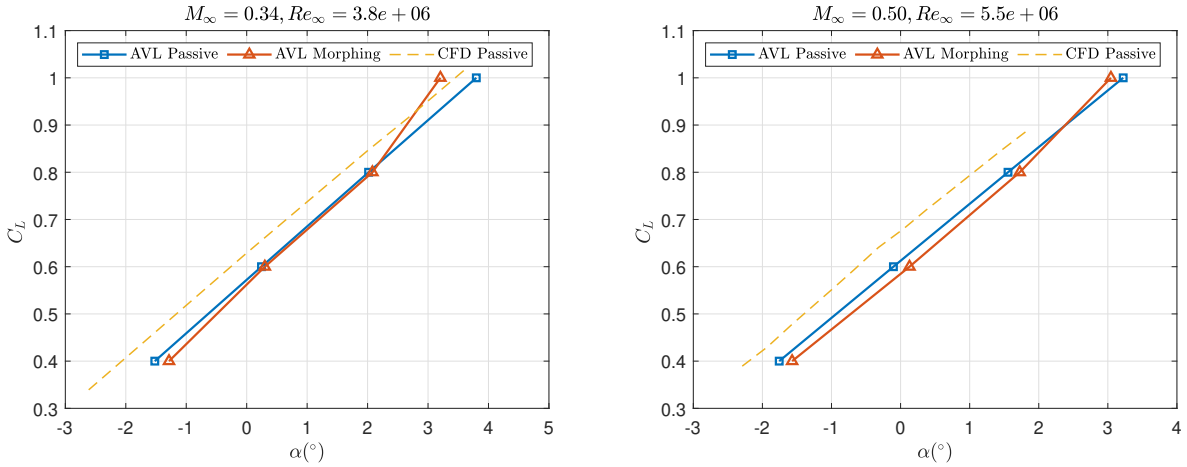

(a) Climb **(b) Cruise**

Fig. 2 AVL and CFD lift coefficient against angle of attack results verification

MSES calculates the 2-D sectional profile drag based on a method combining discrete inviscid Euler and boundary-layer equations suitable for transonic conditions at low Reynolds numbers [34]. Moreover, MSES has also shown good agreement with experimental results in high Reynolds number cases [35], thus, it was considered suitable for the conditions of this study. It should be mentioned that no sweep angle correction was applied since the maximum sweep angle of the wing and the strut were lower than 3° and 5.5° respectively. Lastly, in the strut sections located between the root and the junction, the sectional lift coefficient, c_l was calculated by combining the wing's lift coefficient, c_l^w with the strut's lift coefficient, c_l^{st}, normalized by the ratio of the strut chord, c_{st} to the wing chord, c_w as Eq. 1 indicates.

$$c_l = c_l^w + c_l^{st} \frac{c_{st}}{c_w} \tag{1}$$

Therefore, the sectional profile drag, c_{d_p} which includes both friction and form drag components was computed for each section separately using the c_l from AVL as input. It should be mentioned that the boundary layer transition point was not fixed in the MSES simulations and that wave drag is included in the pressure drag output [31]. Next, the total parasite drag, C_{D_p} of the SBW using as reference the main wing's surface, S and span, b was calculated by integrating the product of the profile drag with the wing chord of each section along the half span (Eq.2).

$$C_{D_p} = \frac{2}{S} \int_0^{\frac{b}{2}} c_{d_p}(y) c_w(y)\, dy \tag{2}$$

Then, the total drag coefficient, C_D can be defined as the sum of the lift-induced drag coefficient, C_{D_i}, calculated by AVL and the total parasite drag, C_{D_p}, computed by MSES as Eq.3 shows.

$$C_D = C_{D_i} + C_{D_p} \tag{3}$$

The number of 2-D sections utilized in this study was determined through a sensitivity analysis, in which the number of sections was gradually increased, and the C_D values were monitored for convergence. In the first iteration, four sections were included: one at the root, one in the middle of the strut's straight part ($y \approx 8.5\ m$) and two sections in the outer wing. During the second iteration, two additional sections were added on either side of the middle section. The final configuration comprised the root section, seven sections from the strut's kink ($y \approx 4\ m$) to the junction, and two sections in the outer wing.

The sensitivity analysis was conducted using the passive strut under all conditions of interest (Table 2). Two typical cases are depicted in Fig. 3, where the total $\Delta C_D\%$ is plotted against the number of sections involved in the integration of Eq. 2. The first iteration was used as reference to calculate the percentage change of C_D. For the climb condition, the total C_D stabilized after eight sections, whereas in cruise the difference between eight and ten sections was less than 0.2%. Therefore, ten sections were used in the optimization process.

As expected, the C_{D_i} remains constant since its value came from the AVL, whereas, the C_{D_p} which is computed by integrating the sectional c_{d_p} values is affected by the number of sections since the vertical distance between the main wing and the strut is changing along the span. A final remark regarding the aerodynamics methodology is that it cannot capture the 3-D effects around the junction, however, the morphing region of the strut, which is the primary focus of this study, starts 1.2 meters away from the junction. Therefore, a significant change in the results is not expected in the case of using high-fidelity 3-D tools.

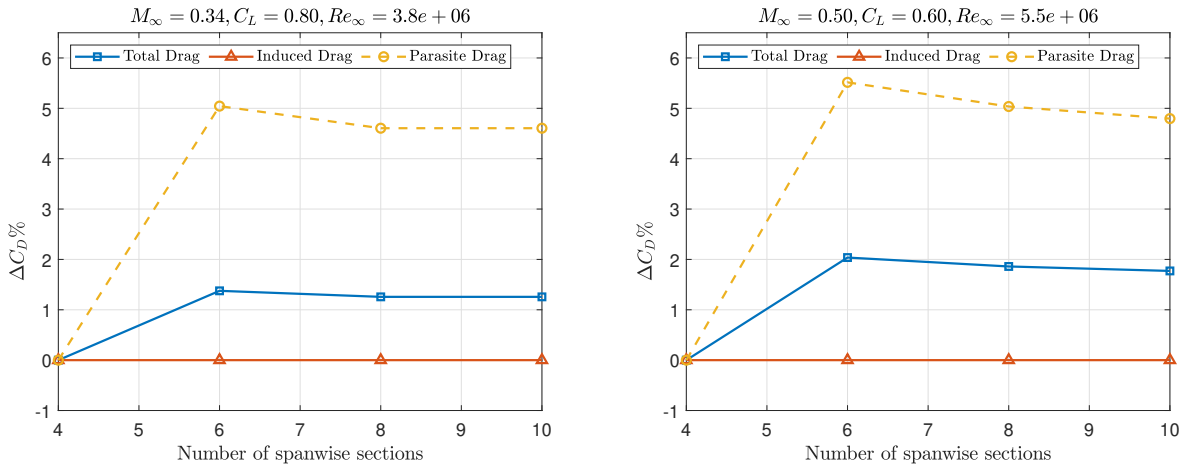

(a) Climb **(b) Cruise**

Fig. 3 Sectional sensitivity analysis of the global drag coefficient

C. Optimization Process

In order to find the aerodynamic shapes that provide the highest aerodynamic efficiency under certain conditions, an optimization study is required [36]. Many optimization algorithms have been used previously in wing shape optimization and are divided in two main categories: the gradient-based and the gradient-free. A well-known gradient-free algorithm is the Genetic Algorithm (GA) which increases the possibility of reaching a global optimum in cases where there is no previous knowledge of the design space. However, it requires significant computational resources compared to the gradient-based algorithms [37].

The design space for this work was unknown, since there is no previous study on applying morphing to the strut of a SBW. Moreover, the Q3D aerodynamic model is characterized by moderate computational demands and only one design variable (δ_{TE}) defines the TE morphing shape of each section as described in Section III.A. Furthermore, no analytical design sensitivities were available to enable the use of a gradient-based optimization algorithm. Hence, the use of a relatively high-cost optimization algorithm was considered a reasonable option. Additionally, the computational time can be reduced even further since the aerodynamic evaluation of a specific member of the population is independent of the other members, allowing it to be conducted in parallel. Therefore, the GA algorithm was selected to perform the optimization of the camber morphing shape of the strut's TE.

The objective function of the optimization was to minimize C_D, with seven strut section δ_{TE} as design variables (Fig. 1), bounded by the maximum deflection values in both directions, as shown in Table 1. The optimization was run separately eight times one for each of the conditions presented in Table 2. These points were selected around the climb and cruise design conditions to examine the aerodynamic benefits of the morphing strut in an off-design environment.

The optimization process is illustrated in Fig. 4. First, the number and the positions of the strut sections used for morphing were determined to meet the minimum requirement of the drag sensitivity analysis (Section III.B), to provide a detailed representation of the TE shape and to account for practical considerations such as the curvature of the strut near its connection points to the fuselage and the wing. Therefore, the regions near the strut root and the wing junction were held undeformed (depicted in black in Fig. 1a).

Table 1 Optimization inputs

	Symbol	Explanation
Objective Function	$min(C_D)$	Minimize C_D in the given conditions
Variables	$X = [\delta_{TE_1}, \delta_{TE_2}, .., \delta_{TE_7}]$	Equivalent TE deflection angle
Bounds	[-8°, 8°]	Minimum and maximum values of δ_{TE}

Second, the initial population of the design variables (δ_{TE}) is randomly initialized by the GA within the design space, which is limited between the bounds presented in Table 1. Each variable value is inserted to the morphing function which generates the corresponding morphed strut geometry of each section. Third, the morphed and fixed sections of the strut are combined with the fixed wing geometry for every member (SBW) of the population. Fourth, the aerodynamic tool described in Section III.B is used to evaluate the objective function. Based on this evaluation the GA creates the next generation of variables, until the convergence criterion (average relative change of objective function equal to 10^{-5}) is met. In summary, the constructed framework permits the single-point optimization of morphing strut's TE shape for each flight condition of Table 2.

Table 2 Optimization conditions

	Mach	C_L
Climb	0.34	[0.4, 0.6, 0.8, 1.0]
Cruise	0.5	[0.4, 0.6, 0.8, 1.0]

IV. Results

The following section includes the GA output after running for 51 generations with 64 members each. The optimum δ_{TE} for each strut section is presented across a range of C_L numbers along with the corresponding drag reduction. Moreover, the effect of the morphing strut on the lift distributions of both wing and strut is discussed. Additionally,

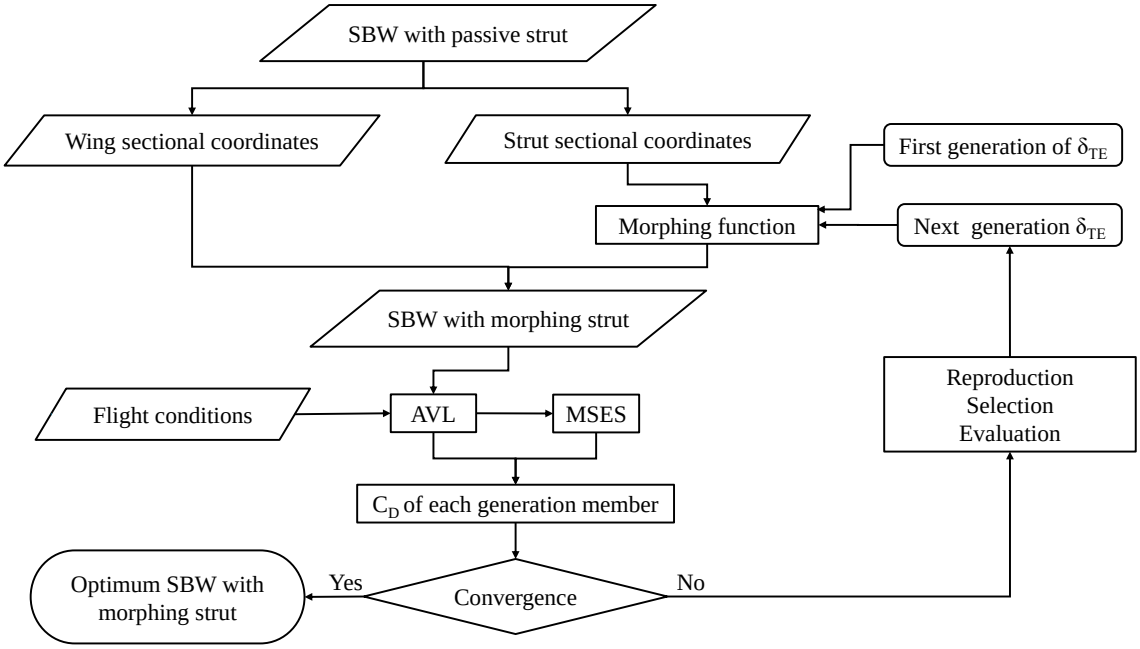

Fig. 4 Optimization flow chart

selected sectional pressure and friction coefficients are depicted to support the explanation of the results.

A. Optimum Equivalent Deflection Angles

The optimized δ_{TE} values for each spanwise section in the eight different conditions of interest are presented in Fig. 5. The overall observation is that the deflection angle becomes more positive, as the section is located closer to the junction with the wing, and as the lift coefficient increases. First, moving from the strut root towards its junction with the wing, the morphing TE exhibits a more positive (clockwise) deflection. Second, there is a significant change in deflection values when C_L increases beyond 0.8. Although, for $C_L \leq 0.8$, the deflection values are close to each other in all sections, at $C_L = 1.0$ there is a strong shift to positive values across the entire strut TE.

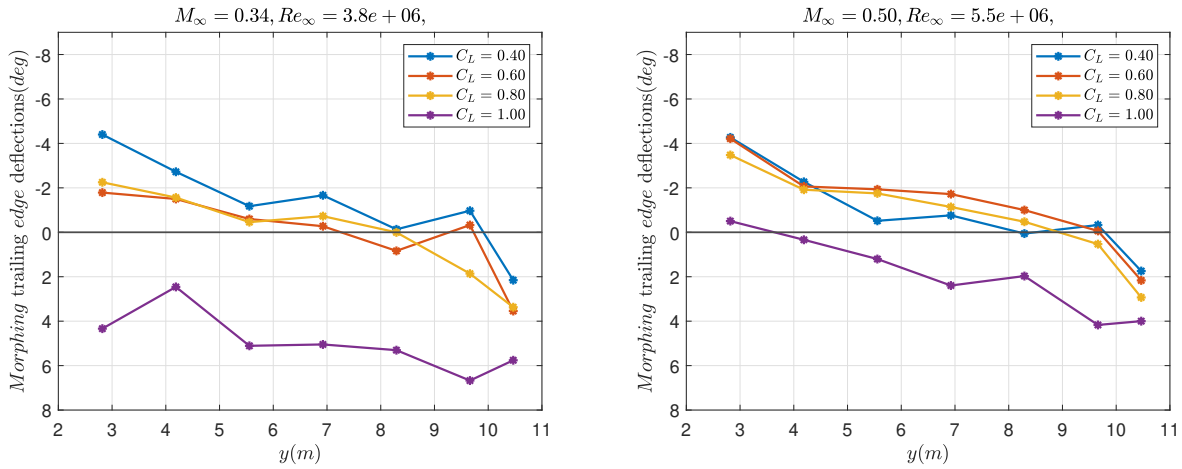

(a) Climb **(b) Cruise**

Fig. 5 Equivalent deflection angles along the strut's span in different lift coefficients

Additionally, the lower magnitude of deflections in both directions shown in cruise compared to climb conditions could be explained by two reasons. First, the higher dynamic pressure in cruise conditions permits the same lift generation with a lower camber change. Second, the SBW geometry with passive strut was optimized by Sticchi et al. [32] for cruise conditions ($M = 0.5, C_L = 0.64$), thus, the shape changes are less extensive in this case.

The above finding contradicts the conclusions of Chau et al.[17] who found that a passive strut should generate positive lift near the fuselage and negative lift near the junction. This difference can be attributed to the different conditions of the two studies. Both studies focus on regional aircraft, however, the configuration in [17] is jet driven with a higher cruise Mach number ($M = 0.78, C_L = 0.68$) and a greater sweep angle ($\Lambda = 30°$) compared to the current study, in which the aircraft is propeller-driven with cruise conditions of $M = 0.5$ and $C_L = 0.64$ and sweep angle of $0° < \Lambda < 5.5°$. Therefore, the compressibility effects near the junction are expected to be more prominent in [17] which could influence the design of the strut shape. Further analysis of the possible factors that affect the current study's results is presented in the next section.

B. Drag Reduction and Spanwise Lift Redistribution

Initially, Fig. 6 indicates that in all examined conditions there is a drag benefit associated with the morphing strut ranging from 0.5% to 3%. Similar to the deflection angles, the trend in C_D reduction between the climb and cruise is comparable. The most distinctive feature is the significant reduction in C_{D_p} at $C_L = 1.0$ in climb, where the entire strut is positively loaded, as depicted in Fig. 7a. This leads to an increase in C_{D_i} as the lift distribution deviates from the elliptical.

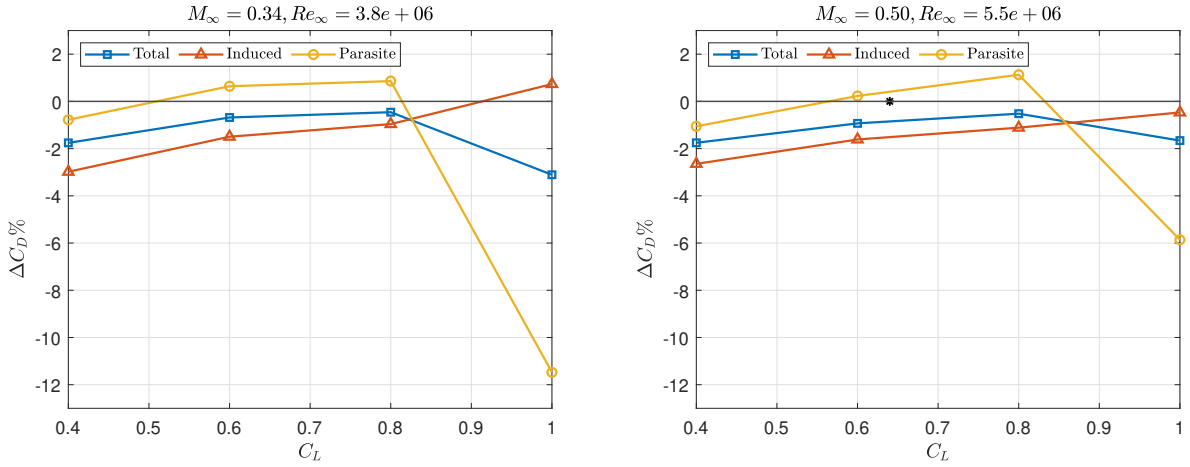

(a) Climb **(b) Cruise**

Fig. 6 Percentage of drag coefficient reduction in different lift coefficients

Nevertheless, this δ_{TE} distribution significantly delays the boundary layer transition on the upper surface of the wing as Fig. 7b shows, which reduces the friction drag coefficient, C_f , thereby decreasing the C_{D_p} sufficiently to compensate for the C_{D_i} increase. A similar behavior, though less pronounced, appears at $C_L = 1.0$ in cruise. Therefore, it is clear that the results of the right part of both diagrams at $C_L = 1.0$ are driven by the laminar-turbulent boundary layer transition since the boundary layer transition location was not specified from the beginning but it was calculated in the 2-D MSES software.

On the left hand side of Fig. 6a, at $C_L = 0.4$ both induced and parasite drag components are decreased. In this case, the morphing TE contributes to a greater negative loading of the strut that leads to a lift distribution close to elliptical (Fig. 8a), hence, the C_{D_i} is 3% lower compared to the passive strut configuration. Regarding the parasite drag, C_{D_p} is also reduced by 1%, resulting in a total benefit of 2% in C_D.

To show the effect of morphing strut on both strut and wing pressure distribution in more detail, the pressure coefficient C_p versus the normalized chord x/c at y = 2.82 m is shown in Fig. 8b. Even in this spanwise location, where the wing and the strut are farther apart, when the lift of the strut becomes negative it tends to reduce the velocity in the region between the wing and the strut thereby causing an increase in the c_l^w mainly by increasing the pressure on the lower side of the wing as depicted in Fig. 8b. However, this effect is also amplified by the increase in the angle of attack

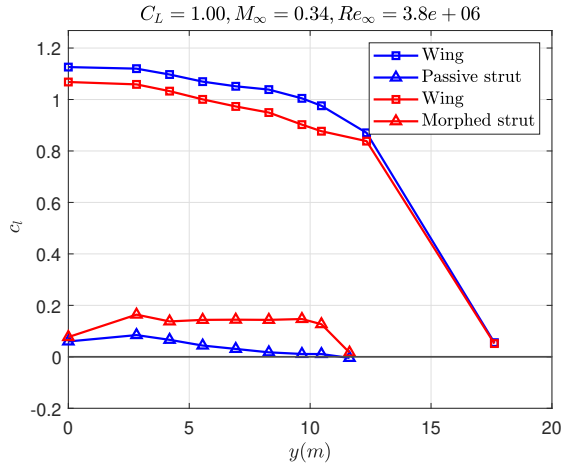

(a) Climb local lift spanwise distribution at C_L = 1

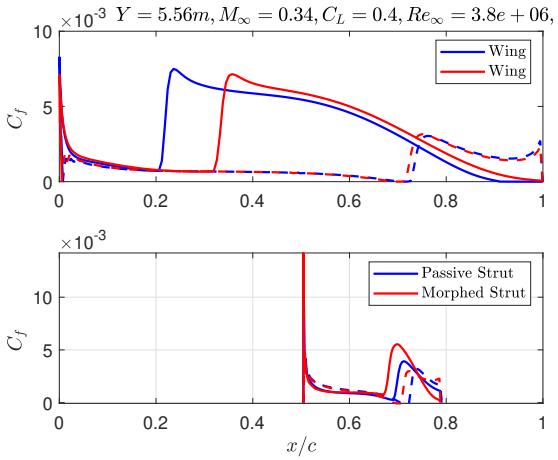

(b) Solid line (suction side) - dashed line (pressure side)

Fig. 7 Local lift coefficient distribution with a selected friction coefficient of one section

of the morphing case. The simulations conducted by keeping the C_L constant and for $C_L \leq 0.8$ the morphing strut SBW had a slightly higher α that the passive strut SBW as demonstrated in Fig. 2. This observation explains why there is also a lower C_p on the upper part of the wing in morphing part case in Fig. 8b. The same reason causes the change in c_l even in the root of SBW where no morphing was implemented.

The findings of this study in this low lift coefficient region ($C_L = 0.4$) align with the results of Secco et al. [16], even if they optimize their passive strut SBW at higher Mach number ($M = 0.78$). This alignment could be attributed to the lower cruise lift coefficient of this study ($C_L = 0.40$) and the smaller sweep angle ($\Lambda = 15°$) compared to Chau et al. [17] who identified a different optimum strut loading.

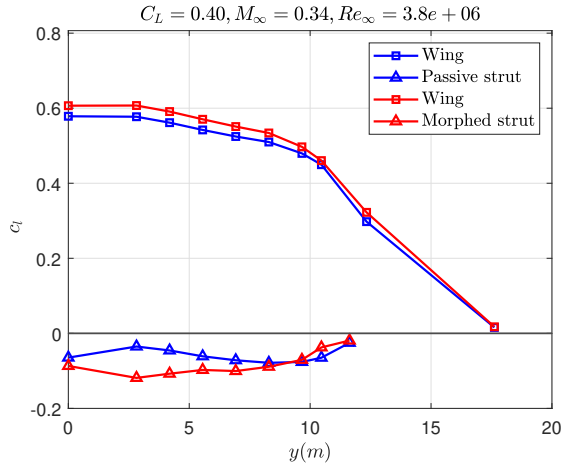

(a) Climb local lift spanwise distribution at C_L = 0.4

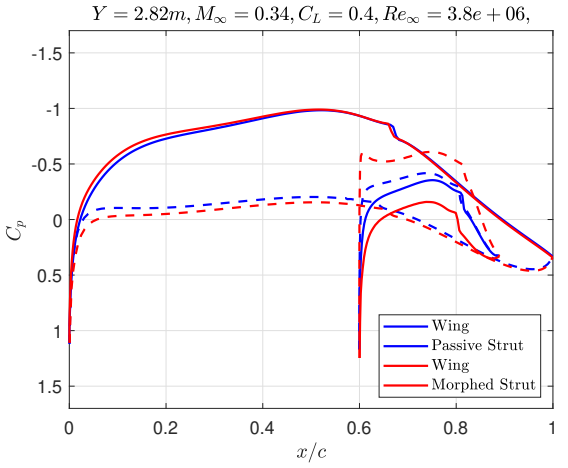

(b) Solid line (suction side) - dashed line (pressure side)

Fig. 8 Local lift coefficient distribution with a selected pressure coefficient of one section

Lastly in the region where $0.6 \leq C_L \leq 0.8$, the GA outputs are closer to the $C_L = 0.4$ than to $C_L = 1.0$ which means that the larger region of the morphing strut is negatively loaded and the drag reduction is dominated by the C_{D_i} decrease. However, there is a C_{D_p} penalty both in climb and cruise in these C_L, which restricts the drag benefits to approximately 1%. The lower drag benefits at the middle C_L values compared to the endpoints were anticipated since the SBW with the passive strut was optimized for a condition closer to them (shown with an asterisk at Fig. 6b), leaving less room for improvement under those conditions.

V. Conclusion

This study explored the application of the camber morphing technology to the TE of the strut of a SBW in order to improve its aerodynamic efficiency by reducing the drag across a range of conditions. This is important because the SBW layout reduces the weight of high aspect ratio wing configurations which is beneficial from an induced drag point of view but also comes with a parasite drag penalty due to the additional surface area of the strut and its interference with the main wing.

In order to obtain the optimum morphing strut TE shapes, an optimization framework was constructed using the GA with the objective of minimizing the drag and seven design variables, the equivalent deflection angle, δ_{TE} of each strut section. The aerodynamic evaluation of each member of the population was conducted by a mid-fidelity Q3D model until the convergence of the algorithm.

The results showed that the camber morphing strut can reduce the C_D from 0.5% to 3% in the examined conditions ($C_L = [0.4, 1.0], M = [0.34, 0.5]$) compared to a passive strut. For $C_L \leq 0.8$ the morphing strut is more negatively loaded than the passive strut, and the drag benefits are caused mainly by the decrease in C_{D_i} , whereas for $0.8 < C_L \leq 1$ the trend changes to positive strut loading and the reduction of C_{D_p} dominates the results.

The next stages of this work are to evaluate the morphing strut concept results at an aircraft level which will require a high-fidelity aerodynamic model to account for complex 3-D flow phenomena near the junction and the connection to the fuselage. Moreover, the final feasibility of the concept will be determined by the trade-off between aerodynamic benefits and the weight penalty of morphing systems.

Acknowledgments

This study is part of the Hybrid Electric Regional Wing Integration Novel Green Technologies project (HERWINGT). This project has received funding from the Clean Aviation Joint Undertaking under the European Union's Horizon Europe research and innovation programme under grant agreement ID 101102010. Views and opinions expressed are however those of the authors only and do not necessarily reflect those of the European Union or the Clean Aviation Joint Undertaking. Neither the European Union nor the granting authority can be held responsible for them.

References

[1] Gern, F. H., Ko, A., Sulaeman, E., Gundlach, J. F., Kapania, R. K., and Haftka, R. T., "Multidisciplinary Design Optimization of a Transonic Commercial Transport with Strut-Braced Wing," *Journal of Aircraft*, Vol. 38, No. 6, 2001, pp. 1006–1014. https://doi.org/10.2514/2.2887.

[2] Ma, Y., and Elham, A., "Designing high aspect ratio wings: A review of concepts and approaches," *Progress in Aerospace Sciences*, Vol. 145, 2024. https://doi.org/10.1016/j.paerosci.2024.100983.

[3] Margetta, R., "New Look at NASA, Boeing Sustainable Experimental Airliner," *NASA*, 2024. URL https://www.nasa.gov/image-article/new-look-at-nasa-boeing-sustainable-experimental-airliner/, (accessed on December 2, 2024).

[4] Cavallaro, R., and Demasi, L., "Challenges, Ideas, and Innovations of Joined-Wing Configurations: A Concept from the Past, an Opportunity for the Future," *Progress in Aerospace Sciences*, Vol. 87, 2016, pp. 1–93. https://doi.org/10.1016/j.paerosci.2016.07.002.

[5] Pfenninger, W., "Design Considerations of Large Global Range High Subsonic Speed LFC Transport Airplanes," *AGARD/VKI Special Course on Concepts for Drag Reduction*, 1977.

[6] Shirley, C. M., Schetz, J. A., Kapania, R. K., and Haftka, R. T., "Tradeoffs of Wing Weight and Lift/Drag in Design of Medium-Range Transport Aircraft," *Journal of Aircraft*, Vol. 51, No. 3, 2014, pp. 904–912. https://doi.org/10.2514/1.C032605.

[7] Nagel, A. L., "Studies of advanced transport aircraft," *NASA*, 1978. URL https://ntrs.nasa.gov/api/citations/19780017104/downloads/19780017104.pdf.

[8] Tetrault, P.-A., Schetz, J. A., and Grossman, B., "Numerical Prediction of Interference Drag of Strut-Surface Intersection in Transonic Flow," *AIAA Journal*, Vol. 39, No. 5, 2001, pp. 857–864. https://doi.org/10.2514/2.1389.

[9] Duggirala, R. K., Roy, C. J., and Schetz, J. A., "Analysis of Interference Drag for Strut-Strut Interaction in Transonic Flow," *AIAA Journal*, Vol. 49, No. 3, 2011, pp. 449–462. https://doi.org/10.2514/1.45703.

[10] Turriziani, R. V., Lovell, W. A., and Martin, G. L., "Preliminary design characteristics of a subsonic business jet concept employing an aspect ratio 25 strut braced wing," *NASA*, 1980. URL https://ntrs.nasa.gov/citations/19780025144.

[11] Gern, F. H., Naghshineh-Pour, A. H., Sulaeman, E., Kapania, R. K., and Haftka, R. T., "Structural Wing Sizing for Multidisciplinary Design Optimization of a Strut-Braced Wing," *Journal of Aircraft*, Vol. 38, No. 1, 2001, pp. 154–163. https://doi.org/10.2514/2.2747.

[12] Gupta, R., Mallik, W., Kapania, R. K., and Schetz, J. A., "Multidisciplinary Design Optimization of Subsonic Strut-Braced Wing Aircraft," *52nd Aerospace Sciences Meeting*, 2014. https://doi.org/10.2514/6.2014-0186.

[13] Bradley, M. K., Droney, C. K., and Allen, T. J., "Subsonic Ultra Green Aircraft Research: Phase II – Volume I – Truss Braced Wing Design Exploration," *NASA*, 2015. URL https://ntrs.nasa.gov/api/citations/20150017036/downloads/20150017036.pdf.

[14] Ting, E., Reynolds, K. W., Nguyen, N. T., and Totah, J., "Aerodynamic Analysis of the Truss-Braced Wing Aircraft Using Vortex-Lattice Superposition Approach," *32nd AIAA Applied Aerodynamics Conference*, 2014. https://doi.org/https://doi.org/10.2514/6.2014-2597.

[15] Carrier, G. G., Arnoult, G., Fabbiane, N., Schotte, J.-S., David, C., Defoort, S., Benard, E., and Delavenne, M., "Multidisciplinary analysis and design of strut-braced wing concept for medium range aircraft," *AIAA SciTech 2022 Forum*, 2022. https://doi.org/https://doi.org/10.2514/6.2022-0726.

[16] Secco, N. R., and Martins, J. R. R. A., "RANS-Based Aerodynamic Shape Optimization of a Strut-Braced Wing with Overset Meshes," *Journal of Aircraft*, Vol. 56, No. 1, 2019, pp. 217–227. https://doi.org/10.2514/1.C034934.

[17] Chau, T., and Zingg, D. W., "Aerodynamic Design Optimization of a Transonic Strut-Braced-Wing Regional Aircraft," *Journal of Aircraft*, Vol. 59, No. 1, 2022, pp. 253–271. https://doi.org/10.2514/1.C036389.

[18] Li, D., Zhao, S., Da Ronch, A., Xiang, J., Drofelnik, J., Li, Y., Zhang, L., Wu, Y., Kintscher, M., Monner, H. P., Rudenko, A., Guo, S., Yin, W., Kirn, J., Storm, S., and Breuker, R. D., "A review of modelling and analysis of morphing wings," *Progress in Aerospace Sciences*, Vol. 100, 2018, pp. 46–62. https://doi.org/10.1016/j.paerosci.2018.06.002.

[19] Bui, T. T., "Analysis of Low-Speed Stall Aerodynamics of a Swept Wing with Seamless Flaps," *34th AIAA Applied Aerodynamics Conference*, 2016. https://doi.org/10.2514/6.2016-3720.

[20] Rivero, A. E., Fournier, S., Manolesos, M., Cooper, J. E., and Woods, B. K. S., "Experimental Aerodynamic Comparison of Active Camber Morphing and Trailing-Edge Flaps," *AIAA Journal*, Vol. 59, No. 7, 2021, pp. 2627–2640. https://doi.org/10.2514/1.J059606.

[21] Abdessemed, C., Bouferrouk, A., and Yao, Y., "Effects of an Unsteady Morphing Wing with Seamless Side-Edge Transition on Aerodynamic Performance," *Energies*, Vol. 15, No. 3, 2022. https://doi.org/10.3390/en15031093.

[22] De Gaspari, A., "Study on the Actuation Aspects for a Morphing Aileron Using an Energy–Based Design Approach," *Actuators*, Vol. 11, No. 7, 2022. https://doi.org/10.3390/act11070185.

[23] Werter, N., Sodja, J., Spirlet, G., and De Breuker, R., "Design and Experiments of a Warp Induced Camber and Twist Morphing Leading and Trailing Edge Device," *24th AIAA/AHS Adaptive Structures Conference*, 2016. https://doi.org/10.2514/6.2016-0315.

[24] De Breuker, R., Mkhoyan, T., Nazeer, N., Stuber, V., Wang, X., Mkhoyan, I., Groves, R., van der Zwaag, S., and Sodja, J., "Overview of the SmartX Wing Technology Integrator," *Actuators*, Vol. 11, No. 10, 2022. https://doi.org/10.3390/act11100302.

[25] Vos, R., Gürdal, Z., and Abdalla, M., "Mechanism for Warp-Controlled Twist of a Morphing Wing," *Journal of Aircraft*, Vol. 47, No. 2, 2010, pp. 450–457. https://doi.org/10.2514/1.39328.

[26] Mkhoyan, T., Thakrar, N. R., De Breuker, R., and Sodja, J., "Morphing wing design using integrated and distributed trailing edge morphing," *Smart Materials and Structures*, Vol. 31, No. 12, 2022. https://doi.org/10.1088/1361-665X/aca18b.

[27] Derksen, R. W., and Rogalsky, T., "Bezier-PARSEC: An optimized aerofoil parameterization for design," *Advances in Engineering Software*, Vol. 41, No. 7-8, 2010, pp. 923–930. https://doi.org/10.1016/j.advengsoft.2010.05.002.

[28] Hileman, J. I., Spakovszky, Z. S., Drela, M., Sargeant, M. A., and Jones, A., "Airframe Design for Silent Fuel-Efficient Aircraft," *Journal of Aircraft*, Vol. 47, No. 3, 2010, pp. 956–969. https://doi.org/10.2514/1.46545.

[29] Drela, M., and Youngren, H., "AVL User Primer - AVL 3.36," *MIT*, 2017. URL https://web.mit.edu/drela/Public/web/avl/, (accessed December 2,2024).

[30] Drela, M., "MSES User's Manual," *MIT*, 2007. URL https://web.mit.edu/drela/Public/web/mses/, (accessed December 2,2024).

[31] Mariens, J., Elham, A., and van Tooren, M. J. L., "Quasi-Three-Dimensional Aerodynamic Solver for Multidisciplinary Design Optimization of Lifting Surfaces," *Journal of Aircraft*, Vol. 51, No. 2, 2014, pp. 547–558. https://doi.org/10.2514/1.C032261.

[32] Sticchi, E., Ragni, D., Casalino, D., and Avallone, F., "Aerodynamic Noise Prediction of Strut-Braced Wing Aircraft," *30th AIAA/CEAS Aeroacoustics Conference*, 2024. https://doi.org/10.2514/6.2024-3012.

[33] Anderson, J., "Fundamentals of Aerodynamics," *McGraw Hill*, 2011.

[34] Drela, M., and Giles, M. B., "Viscous-inviscid analysis of transonic and low Reynolds number airfoils," *AIAA Journal*, Vol. 25, No. 10, 1987, pp. 1347–1355. https://doi.org/10.2514/3.9789.

[35] Fujino, M., Yoshizaki, Y., and Kawamura, Y., "Natural-Laminar-Flow Airfoil Development for a Lightweight Business Jet," *Journal of Aircraft*, Vol. 40, No. 4, 2003, pp. 609–615. https://doi.org/10.2514/2.3145.

[36] Gong, C., and Ma, B.-F., "Shape Optimization and Sensitivity Analysis of a Morphing-Wing Aircraft," *International Journal of Aeronautical and Space Sciences*, Vol. 20, No. 1, 2019, pp. 57–69. https://doi.org/10.1007/s42405-018-0110-7.

[37] Skinner, S. N., and Zare-Behtash, H., "State-of-the-art in aerodynamic shape optimisation methods," *Applied Soft Computing*, Vol. 62, 2018, pp. 933–962. https://doi.org/10.1016/j.asoc.2017.09.030.